Tuning the Magnetic Properties and Structural Stabilities of the 2-17-3 Magnets $Sm_2Fe_{17}X_3$ (X = C, N) by Substituting La or Ce for Sm

Tribhuwan Pandey,* Mao-Hua Du, and David S. Parker†

Material Science and Technology Division, Oak Ridge National Laboratory, Oak Ridge, Tennessee 37831, USA

(Received 17 August 2017; revised manuscript received 18 December 2017; published 5 March 2018)

Designing a permanent magnet with reduced critical rare-earth content is of paramount importance in the development of cost-effective modern technologies. By performing comprehensive first-principles calculations, we investigate the potential avenues for reducing the critical rare-earth content in $Sm_2Fe_{17}N_3$ and $Sm_2Fe_{17}C_3$ by making a La or Ce substitution for Sm. The calculated magnetic properties of base compounds are in good agreement with the previous low-temperature (4.2-K) experimental measurements, and they show a large axial anisotropy. Although La or Ce substitution results in a slight reduction of magnetic anisotropy, the magnetic moments of Fe atoms mostly remain unchanged. Specifically, large axial anisotropies of 7.2 and 4.1 MJ/m^3 are obtained for $SmCeFe_{17}N_3$ and $SmLaFe_{17}N_3$, respectively. These values of anisotropies are comparable to the state-of-the-art permanent magnet $Nd_2Fe_{14}B$. The foremost limitation of $Sm_2Fe_{17}X_3$ magnets for practical application is the formation nitrogen or carbon vacancies at high temperatures. By calculating the N- (C)- vacancy formation energy, we show that La or Ce substitution enhances the vacancy formation energy. This enhanced vacancy formation energy will likely improve the thermodynamic stability of these alloys at high temperatures. Therefore, La- or Ce-substituted $Sm_2Fe_{17}C_3$ and $Sm_2Fe_{17}N_3$ compounds are promising candidates for high-performance permanent magnets with substantially reduced rare-earth content.

DOI: 10.1103/PhysRevApplied.9.034002

I. INTRODUCTION

Permanent magnets are essential for the development of state-of-the-art technologies such as supercomputers, electric cars, and wind turbines, as well as for energy conservation [1–6]. A good permanent magnet requires a large value of magnetization, uniaxial anisotropy, a large coercivity, a high temperature stability, and a high Curie temperature [5,6]. In a permanent magnet, the local atomic moments are favorably aligned along a certain crystallographic direction, which can be characterized by the energy difference versus the other spatial directions. This energy difference is often quantified as the magnetocrystalline anisotropy energy (MAE). The higher MAE usually results in high coercivity, making the demagnetization difficult. The anisotropy mainly arises from the coupling between spin and lattice, also known as spin-orbit coupling [7,8]. Because of the localized nature of rare-earth (R) f electrons, rare-earth-based alloys exhibit a large spin-orbit coupling and, as a consequence, high values of MAE.

Materials based on rare earth (R) and 3d transition metals (T) form a large family of permanent magnets with excellent properties, such as $R_2Fe_{14}B$, RCo_5, R_2Co_{17}, and $R_2Fe_{17}C_y$ compounds [9–15]. The notable example among these classes of R compounds is $Nd_2Fe_{14}B$ [16–22]. The discovery of $Nd_2Fe_{14}B$ has also generated a lot of interest in R_2Fe_{17} compounds. Although the R_2Fe_{17} class of compounds displays large magnetization values, the compounds suffer from low Curie temperatures and planar anisotropy constants. More than two decades ago, Coey and co-workers [23–25] reported that the nitrogenation or carbonation of Sm_2Fe_{17} and Y_2Fe_{17} *switches* the magnetic anisotropy direction from planar to uniaxial and *enhances* their Curie temperature by *2* times. The microscopic origin of this strong ferromagnetism in $Sm_2Fe_{17}N_3$ and $Sm_2Fe_{17}C_3$ has been attributed to the lattice expansion and hybridization between nitrogen (carbon) and iron atoms [26,27]. The (R,Fe)N compounds have been prepared with varying nitrogen stoichiometry [28,29] and show high coercivities of approximately 30 kOe [30]. These developments suggest that the $R_2Fe_{17}N(C)_\delta$ compounds are attractive candidates for permanent magnets.

Although $R_2Fe_{17}N(C)_\delta$ compounds exhibit promising magnetic properties, the resource criticality of R elements such as Nd, Dy, and Sm necessitates the designing of permanent magnets without R elements or with less R content [31]. In this regard, developing a permanent magnet with the use of abundant elements such as La and Ce instead of Sm or Nd [31] could be important for cost

*pandeyt@ornl.gov
†parkerds@ornl.gov

reduction. Another major problem with the technological application of $R_2Fe_{17}N(C)_\delta$ compounds is their stability at high temperatures. $Sm_2Fe_{17}N_3$ ($Sm_2Fe_{17}C_3$) is metastable and decomposes to SmN (SmC) and α-Fe above a temperature of 923 K, making it difficult to fabricate sintered magnets [32,33]. Therefore, improving the stability of $Sm_2Fe_{17}N_3$ (C_3) magnets is another key issue.

In this work, we explore the possibility of reducing the critical R content (Sm) in $Sm_2Fe_{17}N_3$ ($Sm_2Fe_{17}C_3$) by La and Ce substitution for Sm. First, we explore magnetic properties such as magnetic moments and exchange interactions, as well as anisotropy constants for both pristine and La- or Ce-substituted systems. For the base compounds $Sm_2Fe_{17}N_3$ and $Sm_2Fe_{17}C_3$, in agreement with previous experimental studies, we find large axial anisotropies of 13.5 and 3.3 MJ/m^3, respectively. We observe that both $Sm_2Fe_{17}N_3$ and $Sm_2Fe_{17}C_3$ maintain axial anisotropies along with high saturation magnetization even after La or Ce substitution. Specifically, axial anisotropies of 7.2 and 2.7 MJ/m^3 are found for $SmCeFe_{17}N_3$, and $SmCeFe_{17}C_3$, respectively. Next, we explore the effect of La or Ce substitution on the stability of $Sm_2Fe_{17}N_3$ ($Sm_2Fe_{17}C_3$) by calculating N- (C)- vacancy formation energy. The substitution of La or Ce into the lattice significantly improves the stability against nitrogen- (carbon)- vacancy formation, which will improve their stability at high temperatures. Our results indicate that the Sm content in $Sm_2Fe_{17}X_3$ (where X is either N or C) can be reduced by 50% with a slight reduction in magnetic properties. These results chalk out the pathways for the development of alternative magnetic materials with reduced R content, which could be very effective in producing low-cost permanent magnets.

II. COMPUTATIONAL APPROACH

Calculations are performed using the all-electron density-functional-theory code WIEN2K [34–36] together with the generalized-gradient approximation of Perdew, Burke, and Ernzerhof [37]. The sphere radii are set at 2.50, 1.88, 1.61, and 1.61 bohr for Sm, Fe, N, and C. For good convergence, a $RK_{\max}$ value (the product of the smallest sphere radius and the largest plane-wave expansion wave vector) of 7.0 is used. All calculations are performed with the experimental lattice parameters [38–40], and all internal coordinates are relaxed until forces on all of the atoms are less than 1 mRy/bohr. Experimental lattice parameters along with the generalized-gradient approximation (GGA)-optimized lattice parameters are shown in Table I. The GGA-optimized lattice parameters are in nice agreement with the experiments. We also check the dependence of optimized lattice parameters on the Hubbard U. The lattice parameters are found to be very sensitive to the U value used; hence, in order to model a reliable system, all of the computations presented in this work are done with the experimental lattice parameters. For La or Ce substitution for Sm, one out of two Sm atoms in the primitive cell is replaced by La or Ce. These substituted structures are subsequently relaxed to their ground states by minimizing the forces on all of the atoms. For the structure relaxation, 1000 **k** points are used in the full Brillouin zone. Upon going from $Sm_2Fe_{17}N_3$ ($Sm_2Fe_{17}C_3$) to $Ce_2Fe_{17}N_3$ ($Ce_2Fe_{17}C_3$), the cell volume varies nominally by 0.2% (0.4%); hence, for the substituted compounds, the lattice parameter is fixed at the corresponding values for parent nitrides and carbides.

TABLE I. The experimental a and c lattice parameters (marked as Exp.), along with the DFT-optimized lattice parameters (within the GGA) for Sm_2Fe_{17}, $Sm_2Fe_{17}N_3$, and $Sm_2Fe_{17}C_3$. All of the calculations reported in this work are performed with the experimental lattice parameters.

	Exp.		GGA	
Compound	a (Å)	c (Å)	a (Å)	c (Å)
Sm_2Fe_{17}	8.558 [40]	12.441 [40]	8.55	12.46
$Sm_2Fe_{17}N_3$	8.743 [39]	12.659 [39]	8.70	12.68
$Sm_2Fe_{17}C_3$	8.744 [38]	12.572 [38]	8.70	12.53

All of the calculations are performed by assuming a collinear spin arrangement. The MAE is obtained by calculating the total energies of the system with spin-orbit coupling (SOC) as $K = E_a - E_c$, where E_a and E_c are the total energies for the magnetization oriented along the a ($11\bar{2}$ in a rhombohedral primitive cell) and c (111 in a rhombohedral primitive cell) directions, respectively. A positive (negative) K value corresponds to uniaxial (planar) anisotropy. Although the calculation of MAE from first-principles methods is somewhat difficult, as shown in some recent studies [22,41–45], precise calculations often produce a MAE that is in good agreement with experiments. To ensure the accuracy of the MAE, its convergence with respect to the number of **k** points is carefully checked. The difference in MAE calculated using 2000 and 3000 **k** points is less than 1.5%, as shown in Fig. 1(a). All of the MAE values reported in this paper correspond to 2000 reducible **k** points in the full Brillouin zone.

A number of different methodologies have been developed for the accurate treatment of the correlated nature of R f electrons. For example, the self-interaction-corrected local-spin-density scheme [46,47] can provide insight into localized and bandlike features of f electrons. Alternately, the density-functional theory with the Hubbard U parameter (DFT + U) approach introduces an effective Hubbard U parameter that separates the f bands into lower and upper Hubbard bands. Here, the strong interactions between the Sm and Ce f electrons are included by incorporating a Hubbard U correction. The U value for the Sm site is obtained by optimizing the various magnetic properties (MAE, magnetic moments) with respect to the available experimental data. The obtained U values lie in the typical range that has been used before to correctly describe the

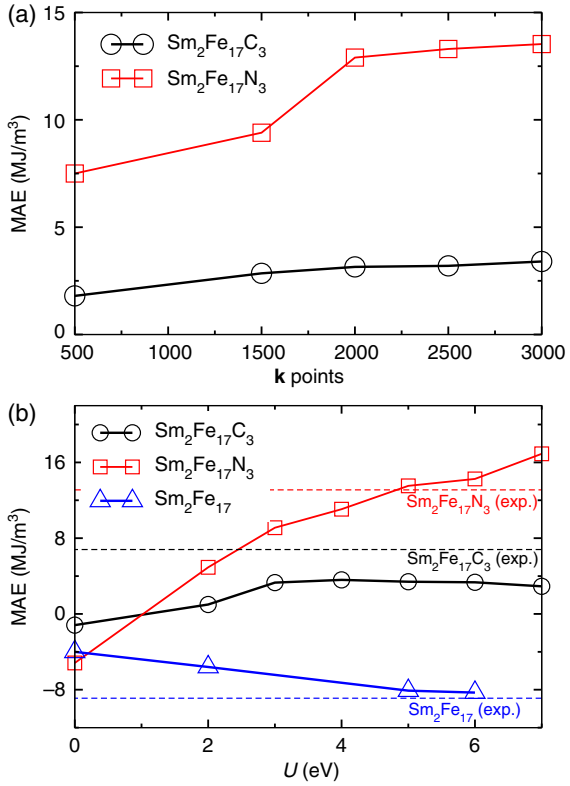

FIG. 1. (a) The dependence of magnetocrystalline anisotropy energy (MAE) on the number of **k** points used. The **k**-point convergence is checked at $U = 6$ eV. (b) The Hubbard U dependence of the calculated MAE values for $Sm_2Fe_{17}N_3$, $Sm_2Fe_{17}C_3$, and Sm_2Fe_{17}. Experimental values are also marked, for comparison, with dashed lines. These calculations are performed by taking 2000 reducible **k** points in the Brillouin zone.

magnetic properties of Sm-based compounds [44,48–50]. The convergence of MAE for $Sm_2Fe_{17}N_3$ and $Sm_2Fe_{17}C_3$ with respect to the U parameter is shown in Fig. 1(b). In order to optimize the U value for Ce-substituted compounds (i.e., for $SmCeFe_{17}N_3$ and $SmCeFe_{17}C_3$), we calculate the MAE by varying the U value at the Ce site for a fixed U_{Sm} value, which is shown in Figs. 2(a) and 2(b). On varying U_{Ce} from 3 to 6 eV, the MAE varies by $< 10\%$ for both of the

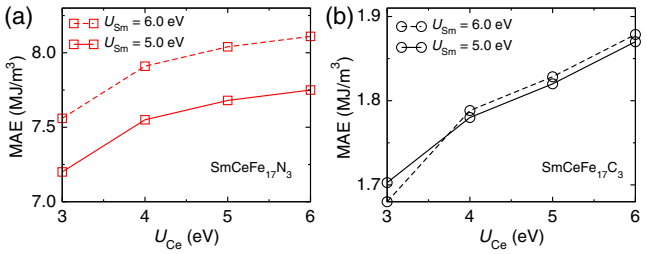

FIG. 2. The dependence of the calculated MAE values for (a) $SmCeFe_{17}N_3$ and (b) $SmCeFe_{17}C_3$ on the Hubbard U parameter on a Ce site at a fixed U_{Sm}. Upon varying U_{Ce} from 3 to 6 eV, the MAE varies by $< 10\%$.

systems. All of the calculations presented in this work are done with $U_{Sm} = 6.0$ eV and $U_{Ce} = 3.0$ eV, with the Hund's coupling parameter J as zero. The addition of the Hubbard U requires the double-counting correction terms in the energy functional to account for the fact that the Coulomb energy is already included in the DFT functional. To this end, here the self-interaction correction scheme [51–53] (also known as the fully localized limit) [44,54] is used, where the on-site Coulomb interaction for localized orbitals is parametrized by $U_{\text{effective}} = U - J$. It is important to mention that, due to the presence of localized f orbitals, DFT + U calculations for R-based compounds may often converge in a metastable state. Hence, to find the actual ground state, different starting configurations with varying f-orbital occupancies are used. After a self-consistent cycle, the system always converges to complex m states (pure atomic m states were never reached). As our calculated magnetic moments and other properties are in reasonable agreement with the experiments, we assume that we have an actual ground state.

For the nitrogen- or carbon-vacancy formation-energy calculations, a 66-atom unit cell (UC) is used for both $Sm_2Fe_{17}N_3$ and $Sm_2Fe_{17}C_3$. This large unit cell provides enough distance between the periodic images of the nitrogen or carbon vacancies, with the in-plane distance being 8.74 Å and the out-of-plane distance being 12.57 Å. Full structural relaxations of internal positions for pristine (defect-free) unit cells and unit cells with nitrogen or carbon vacancies are performed until the residual forces are smaller than 2 mRy/bohr. The calculations converge on a $4 \times 4 \times 4\Gamma$-centered **k**-point grid that includes spin polarization. For all of the vacancy calculations, the lattice parameters are fixed at the corresponding values for parent nitrides and carbides. These calculations are also performed using WIEN2K code. The formation energy of the N or C vacancy (ΔE_f) is defined as follows:

$$\Delta E_f = E_{\text{UC}}^{\text{N(C)vac}} - E_{\text{UC}}^{\text{pristine}} + E_{\text{N(C)}}, \qquad (1)$$

where, $E_{\text{UC}}^{\text{N(C)vac}}$ denotes the energy of a unit cell with a nitrogen or carbon vacancy, $E_{\text{UC}}^{\text{pristine}}$ is the energy of the pristine unit cell, and the last term is the total energy per atom for nitrogen or carbon. Here, a N_2 molecule and graphite are used as a reference to obtain the total energy for the nitrogen and carbon atoms. The formation-energy values are also recalculated by including spin-orbit coupling and the Hubbard U. Note that due to the computation cost we only checked one 50-50 Sm and Ce (La) configuration in the unit cell, keeping the local environment around the vacancy equivalent [with respect to equal numbers of Sm and Ce (La) nearest neighbors] in all the cases. The defect formation energy may vary slightly depending upon the configuration of Sm and Ce (La) in the unit cell.

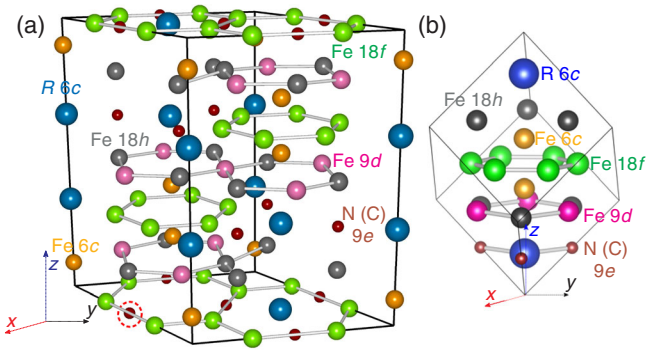

FIG. 3. (a) Crystal structure of the rhombohedral (Th_2Zn_{17}-type) allotropes of $Sm_2Fe_{17}X_3$. (a) 66-atom unit cell. (b) 22-atom primitive cell along with the crystallographic directions mapped according to the unit cell. All nonequivalent crystallographic sites are also marked by the corresponding atom color. The circled red atom denotes the N (C) atom removed for modeling a cell with N (C) vacancy.

III. RESULTS AND DISCUSSION

The R_2M_{17} allotropes exist in two different crystal structures; the rhombohedral Th_2Zn_{17}-type and the hexagonal Th_2Ni_{17}-type structure. The rhombohedral structure is stable for the light R elements (from Ce to Eu), whereas, for the heavy R elements (from Gd to Lu), the hexagonal structure is most stable. As shown in Figs. 3(a) and 3(b), the Th_2Zn_{17} structure is a layered structure built from close-packed Fe layers alternating with mixed layers of R-Fe. The elements with small atomic radii, such as nitrogen, carbon, and hydrogen, occupy the interstitial sites ($9e$) as shown in Fig. 3(a), which in turns improves the magnetic properties of these compounds [38,39].

To check the stable ground state, calculations are performed for three different magnetic configurations: (i) R atoms are aligned with respect to Fe atoms (FM), (ii) R atoms are antialigned with respect to Fe atoms (AFM), and (iii) a nonmagnetic (NM) configuration is used. The corresponding energies with respect to the NM state are listed in Table II. For all three systems, Sm_2Fe_{17}, $Sm_2Fe_{17}N_3$, and $Sm_2Fe_{17}C_3$, we find the ground state to have a Sm spin moment opposite that of the Fe one, with an energy costs relative to the Fe-Sm NM alignment determined as 759.3, 850, and 789 meV per Fe atom. These energies can be used to compute the R-Fe exchange couplings (J_{RM}) within the two-sublattice model. Within this model, the J_{RM} is defined as [55,56]

$$J_{RM} = \frac{E_{\mathrm{AFM}} - E_{\mathrm{FM}}}{4 S_R S_{\mathrm{Fe}} Z_R Z_{\mathrm{Fe}}}. \quad (2)$$

Here, E_{AFM} and E_{FM} are the total energies of the ferromagnetic and antiferromagnetic configurations. S_R and S_{Fe} are the spin moments of the R and Fe sublattices, respectively. For these calculations, S_{Fe} is averaged over four crystallographically nonequivalent Fe sites. Z_{Fe} and Z_R are the number of nearest-neighboring Fe atoms around the R atom and the number of R elements in the simulation cell, respectively. The above expression leads to a Sm-Fe exchange coupling parameter (J_{RM}) of -1.9, -1.3, and -1.3 meV for Sm_2Fe_{17}, $Sm_2Fe_{17}N_3$, and $Sm_2Fe_{17}C_3$, as shown in Table II. For $Sm_2Fe_{17}C_3$ and $Sm_2Fe_{17}N_3$, we see a slight reduction in J_{RM} in comparison to Sm_2Fe_{17}. A similar value of J_{RM} has been reported for the $R_2Fe_{14}B$ family of magnets [55,57,58].

The magnetic moments for Sm_2Fe_{17} and its nitride ($Sm_2Fe_{17}N_3$) and carbide ($Sm_2Fe_{17}C_3$) are shown in Fig. 4(a) and summarized in Table III. Our calculated magnetic moments and those obtained from other electronic structure calculations for the parent compound Sm_2Fe_{17} and its nitride and carbide [27,56,59,60] show good qualitative agreement. The quantitative comparison is a bit difficult, as these calculations differ in the treatment of the $4f$ electrons [27,56,61], lattice parameters, and atomic positions. The calculated Fe orbital moments for Sm_2Fe_{17}, which are shown in Table III in parentheses, lie between $0.04\mu_B$ and $0.05\mu_B$. The Fe orbital moments are enhanced when interstitial nitrogen or carbon is inserted, and the enhancement is higher for $Sm_2Fe_{17}C_3$. Furthermore, on introducing nitrogen or carbon interstitial atoms, while the spin moments of Fe $18f$ and Fe $18h$ sites—which are close to N or C atoms—are slightly decreased, the moments on the more distant Fe $9d$ site are enhanced, as shown in Table III and in Figs. 5(a) and 5(b). This trend of Fe moments in nitrogenation or carbonation is in good qualitative agreement with previous studies and has been attributed to hybridization between N (C) and Fe atoms [26,27]. Regardless of this slight variation, the average Fe spin moment in these systems remains in the range of $(2.36–2.44)\mu_B$, which is significantly higher than the value for bcc Fe $2.2\mu_B$. The Sm total magnetic moments are also listed in Table III and displayed in Fig. 4(a). The variations in the Sm orbital and the spin magnetic moments for both $Sm_2Fe_{17}N_3$ and $Sm_2Fe_{17}C_3$ are shown in Fig. 6. The calculated orbital moment of Sm atoms without U is rather small ($1.58\mu_B$ for $Sm_2Fe_{17}N_3$ and $1.79\mu_B$ for $Sm_2Fe_{17}C_3$). Upon varying U in GGA + SOC + U calculations, the orbital moment of Sm atoms increases rapidly and saturates

TABLE II. The calculated relative energies per Fe atom for ferromagnetic (FM) and antiferromagnetic (AFM) arrangements of Fe atoms with respect to R atoms. The presented energies are calculated with respect to nonmagnetic (NM) configuration on per Fe atom basis.

Compound	E_{NM} (meV)	E_{FM} (meV)	E_{AFM} (meV)	J_{RM} (meV)
Sm_2Fe_{17}	0	−684.3	−759.3	−1.9
$Sm_2Fe_{17}N_3$	0	−802.0	−850.0	−1.3
$Sm_2Fe_{17}C_3$	0	−746.0	−789.0	−1.3

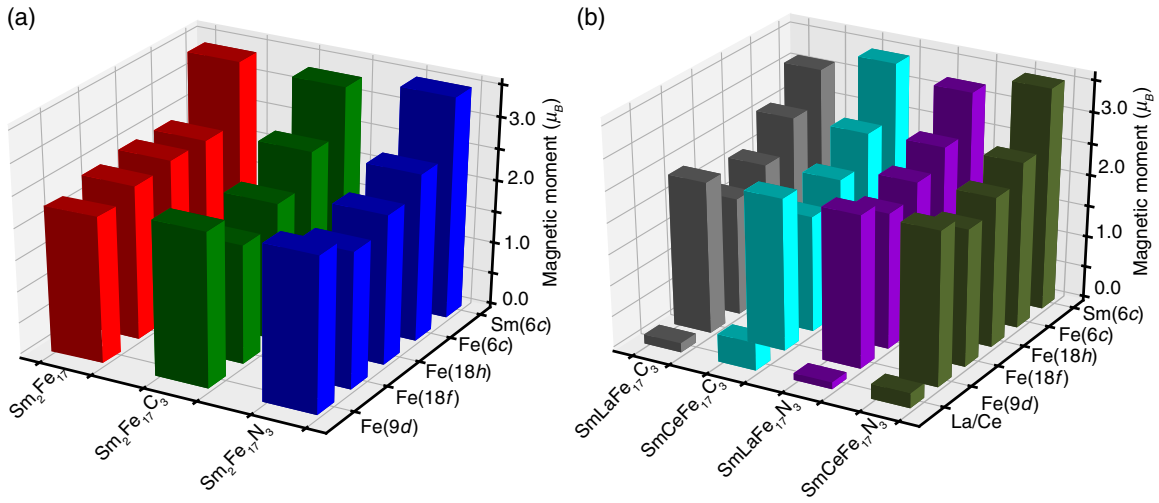

FIG. 4. The calculated total (orbital plus spin) magnetic moments at various nonequivalent atomic sites for (a) pristine and (b) La- or Ce-substituted systems. The calculated magnetic moments of R atoms are negative and are shown here as positive.

TABLE III. Calculated total (orbital plus spin) magnetic moments at various atom sites in μ_B, the total magnetic moment of the system (m_{tot}) in μ_B per formula unit, the saturation magnetization (M_S) in tesla, and the magnetocrystalline anisotropy constant (K_1) in MJ/m^3 for Sm_2Fe_{17}, $Sm_2Fe_{17}X_3$, $SmLaFe_{17}X_3$, and $SmCeFe_{17}X_3$. The corresponding orbital moments are shown in parentheses. Here, X represents carbon or nitrogen atoms. These values are calculated while including SOC with magnetization along the [001] (111 in rhombohedral coordinates) direction with U values of 6 and 3 eV at the Sm and Ce sites, respectively. Comparison of the calculated and the experimental total magnetization (in μ_B per formula unit) and K_1 (in MJ/m^3) is also shown. The contribution of R atoms to the MAE is quantified by calculating the MAE while applying spin-orbit coupling only at R atoms (K_1^R). Nearly 75% of the MAE originates from R atoms. For comparison, the state-of-the-art permanent magnet $Nd_2Fe_{14}B$ [21,68] exhibits K_1 of 4.9 MJ/m^3 and m_{tot} of 37.7μ_B/f.u.

	R-Fe	(R,Fe)N			(R,Fe)C		
Atom site	Sm_2Fe_{17}	$Sm_2Fe_{17}N_3$	$SmLaFe_{17}N_3$	$SmCeFe_{17}N_3$	$Sm_2Fe_{17}C_3$	$SmLaFe_{17}C_3$	$SmCeFe_{17}C_3$
$X(9e)$		−0.05	−0.04	−0.043	−0.15	−0.15	−0.15
Fe($9d$)	2.19(0.047)	2.48(0.053)	2.45(0.038)	2.48(0.05)	2.46(0.054)	2.43(0.048)	2.44(0.047)
Fe($18f$)	2.44(0.041)	2.17(0.043)	2.18(0.034)	2.20(0.04)	1.89(0.047)	1.88(0.041)	1.86(0.040)
Fe($18h$)	2.43(0.047)	2.37(0.056)	2.38(0.053)	2.40(0.058)	2.18(0.059)	2.14(0.058)	2.16(0.060)
Fe($6c$)	2.66(0.049)	2.65(0.060)	2.65(0.046)	2.66(0.05)	2.65(0.068)	2.62(0.058)	2.62(0.056)
$R(6c)$	−3.40(2.33)	−3.53(2.27)	−3.24(2.25)	−3.54(2.24)	−3.33(2.35)	−3.13(2.32)	−3.46(2.36)
La or Ce			−0.11(0.005)	−0.24(0.66)		−0.15(0.002)	−0.45(0.52)
m_{tot}	34.0	33.0	36.2	35.9	29.5	32.6	31.9
$m_{\text{tot}}^{\text{exp}}$	35.9[a]	38.2[b]			34.5[c]		
M_S (T)	1.47	1.37	1.51	1.50	1.24	1.37	1.34
M_S^{exp} (T)	1.03–1.20[d]	1.54–1.57[e]			1.45[f]		
K_1	−8.9	13.5	4.1	7.2	3.4	1.2	1.7
K_1^{exp}	−8.1[g]	13.1[h]			6.9[i]		
K_1^{Rj}	−6.9	10.5	3.5	5.3	2.3	1.0	1.2

[a] Sm_2Fe_{17} [62].
[b] $Sm_2Fe_{17}N_{2.7}$ [1].
[c] $Sm_2Fe_{17}C_{2.3}$ [63].
[d] Sm_2Fe_{17} [23,29].
[e] $Sm_2Fe_{17}N_3$ [64,65].
[f] $Sm_2Fe_{17}C_3$ [65].
[g] Sm_2Fe_{17} [66].
[h] $Sm_2Fe_{17}N_{2.6}$ [67].
[i] $Sm_2Fe_{17}C_2$ [67].
[j] MAE calculated by incorporating spin-orbit coupling only at the Sm, Ce, and La sites.

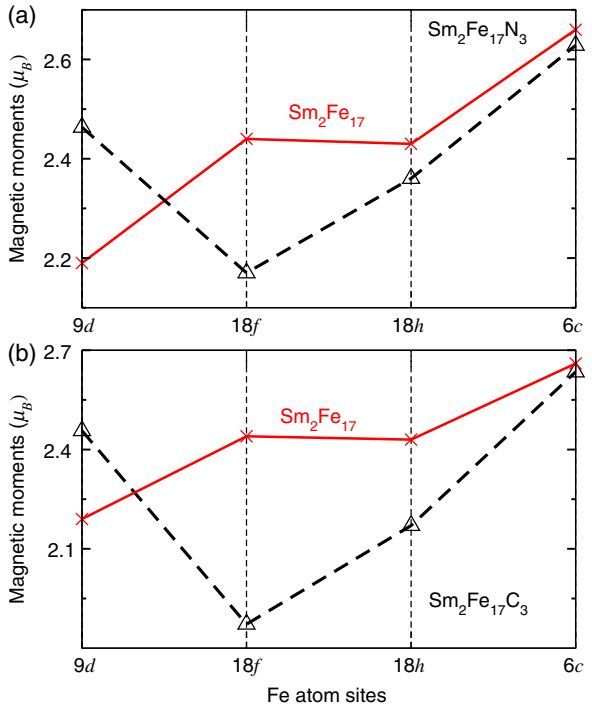

FIG. 5. The calculated total (spin plus orbital) magnetic moments on Fe sites for (a) $Sm_2Fe_{17}N_3$ and (b) $Sm_2Fe_{17}C_3$. The total magnetic moments of various Fe sites in Sm_2Fe_{17} are also shown for comparison. Total (spin plus orbital) magnetic moments on various Fe sites remain independent of the U_{Sm} value used, and the main impact of U is only at MAE.

at higher values of U. The rate of increase of orbital moments with U is higher for a nitrogen interstitial compound than a carbon interstitial compound. The variation of Sm spin moments with the U parameter is also shown in the inset of Fig. 6. As expected, the Sm spin moments display very weak dependence on the U values. For $U_{Sm} = 6$ eV, we see that Sm atoms have large

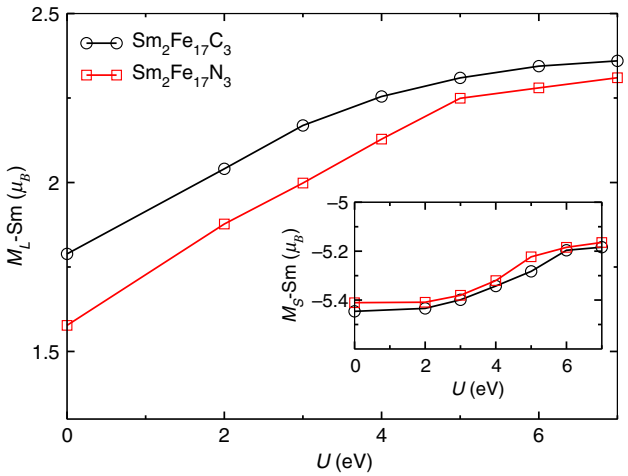

FIG. 6. U dependence of Sm orbital and spin (inset) magnetic moments for $Sm_2Fe_{17}N_3$ and $Sm_2Fe_{17}C_3$.

(approximately $2.3\mu_B$) orbital moments. For C interstitial compounds, the orbital moment of Sm remains unchanged; however, it slightly decreases in the case of the N interstitial. The magnetic moment for La- or Ce-substituted compounds can be found in Fig. 4(b) and Table III. As can be seen for the substituted compounds, the magnetic moments on Fe and Sm sites remain more or less unchanged. On the other hand, the magnetic moments on the substituted R atomic sites (La and Ce) are quenched, as La has no f electrons and Ce has only one outermost f electron.

The total magnetization in the parent, interstitial, and La- or Ce-substituted compounds is summarized in Table III. For the Sm_2Fe_{17} and interstitial compounds, the calculated total magnetic moment agrees well with the experimental measured value determined by neutron diffraction [69,70] or magnetization measurements at low temperature [1,63,71,72]. We obtain saturation magnetic moments of 1.2 and 1.4 T for $Sm_2Fe_{17}C_3$ and $Sm_2Fe_{17}N_3$, respectively, which is in fair agreement with the experimentally measured 4.2 K value shown in Table III. Considering the notable difficulties associated with modeling of R elements with first-principles methods, this agreement is quite reasonable. Another reason for the deviation between the calculated and measured data could be the nonstoichiometric effects. Owing to the reduced (negative) magnetic moment at the La and Ce sites, we see enhanced total magnetic moments for the substituted compounds in comparison to $Sm_2Fe_{17}C_3$ and $Sm_2Fe_{17}N_3$.

Next, we turn our attention to the MAE constant K_1, which is shown in Fig. 7 and Table III. The MAE represents the energy required for changing the orientation of the magnetic moments under the application of a magnetic field. The MAE is an essential quantity for achieving high coercivity in a permanent magnet. The MAE value calculated without a U parameter does not agree with the

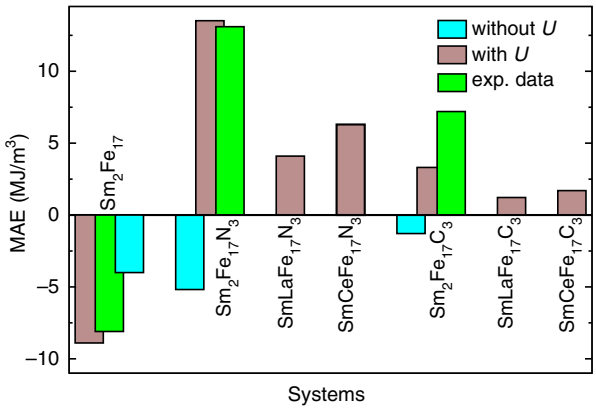

FIG. 7. The calculated magnetocrystalline anisotropy energy (MAE) for Sm_2Fe_{17}, $Sm_2Fe_{17}N_3$, $Sm_2Fe_{17}C_3$, and La- or Ce-substituted systems when including U parameters of 6 eV at the Sm site and 3 eV at the Ce site. The experimental MAE (the filled green bars) and MAE values obtained without a U parameter (the filled cyan bars) are also shown for comparison.

experiments. In fact, as shown in Fig. 7, even the sign of the MAE cannot be predicted correctly. This indicates that, in these systems, correlation in Sm and Ce atoms is very important, and therefore we apply a on-site U parameter to both Sm and Ce that tends to localize the f electrons. The effect of the on-site Hubbard U parameter on the MAE is clear from the GGA+U calculations, which are shown in Fig. 1(b). $Sm_2Fe_{17}C_3$ and $Sm_2Fe_{17}N_3$ exhibit quite different levels of dependence on the U parameter. While, for $Sm_2Fe_{17}N_3$, the MAE exhibits a strong dependence on U, the U dependence of the MAE for $Sm_2Fe_{17}/Sm_2Fe_{17}C_3$ is rather weak. This indicates that, for R magnets, electron correlations play a central role in producing large MAE values (coercivity), and it explains why local-density-approximation and GGA calculations often underestimate the MAE of R magnets. We find the parent compound Sm_2Fe_{17} to be planar, with a K_1 value of -8.9 MJ/m^3, whereas a large positive MAE value is seen for the C and N interstitial compounds. The positive sign for K_1 means that, as observed experimentally, the material is easy axis, which is favorable for permanent-magnet applications. Also, the magnitude of K_1 is significantly higher than the value of 2 MJ/m^3 that is a key requirement for high-performance permanent magnets [5,6]. Specifically, large axial anisotropies of 3.3 and 13.5 MJ/m^3 are obtained for $Sm_2Fe_{17}C_3$ and $Sm_2Fe_{17}N_3$, respectively. The measured anisotropy values from previous experimentally studies are also listed in Table III. Overall there is fair agreement between the calculated and measured values. The discrepancy between theory and experiment can be associated with the non-stoichiometry of N or C in the experimental samples.

The MAE in R-T magnets originates mainly from two sources: (i) the MAE of the Fe sublattice and (ii) the single-site anisotropy of the Sm f orbitals due to strong spin-orbit coupling and crystal-field effects [73–75]. In order to decouple the contribution to the MAE from R and the Fe sublattice, we run the anisotropy calculation by switching off the spin-orbit coupling at Fe sites, which is represented by K_1^R in Table III. We see that the contribution of R atoms to the MAE is more than 75%. This result is in agreement with the experiments, where it is shown that most of the low-temperature anisotropy originates from the R sublattice [1]. The experimental observation of the switching of the MAE from easy plane to easy axis for interstitial compounds is nicely reproduced by our calculations. As noted in Refs. [27,75], this switching of the MAE sign can be explained on the basis of a crystal field. The second-order crystal-field parameter (A_2^0) which determines the trend of the MAE in R magnets is significantly increased upon insertion of interstitial N or C, which helps switch the direction of the MAE from easy plane to easy axis. A similar mechanism has been proposed for explaining the higher MAE values of $SmCo_5$. As noted by Larson and co-workers [44,74] for $SmCo_5$ and related compounds, the comparable strength of crystal-field and spin-orbit effects results in a large MAE value for these compounds. At the same time, the substantially weaker crystal-field effect results in a relatively smaller anisotropy in Sm_2Co_{17}.

We next evaluate the effect of the La or Ce contribution to the MAE, which is shown in Fig. 7 and Table III. While, for Ce-substituted compounds, the reduction in the MAE is roughly proportional to the substituted Sm atoms, a higher reduction in the MAE is observed for La-substituted compounds. For example, in the cases of $SmCeFe_{17}N_3$ and $SmLaFe_{17}N_3$, the MAE is reduced by 40% and 70%, respectively. Although the MAE is somewhat reduced after La or Ce substitution, it still maintains a large positive value. Specifically, large axial anisotropies of 7.2 and 4.1 MJ/m^3 are obtained for $SmCeFe_{17}N_3$ and $SmLaFe_{17}N_3$, respectively, which are comparable to $Nd_2Fe_{14}B$ (4.9 MJ/m^3) [21,68]. These results thus indicate that the La- and Ce-substituted systems could be promising for permanent-magnet applications. Unlike $Sm_2Fe_{17}N_3$ and $Sm_2Fe_{17}C_3$, for Ce-substituted compounds, the experimental data of the MAE is not available; hence, a *proper* U cannot be estimated by fitting the MAE to the experimental data. In order to optimize the U value for Ce-substituted compounds (i.e., for $SmCeFe_{17}N_3$ and $SmCeFe_{17}C_3$), we calculate the MAE by varying U at the Ce site for a fixed U_{Sm} value, which is shown in Figs. 2(a) and 2(b). Upon varying U_{Ce} from 3 to 6 eV, the MAE varies only by <10% between the two systems, and all of the calculations reported here are done with U_{Ce} at 3 eV. Based on this analysis, we conclude that our results are not very sensitive with respect to U_{Ce}.

The density of states (DOS) for crystallographically nonequivalent Fe atoms in Sm_2Fe_{17} and $Sm_2Fe_{17}N_3$ is shown in Figs. 8(a)–8(d). Similar information for $Sm_2Fe_{17}C_3$ is given in Fig. 9. The DOS depicts behavior of a typical ferromagnetic system. Partial densities of states for R atoms are compared in Fig. 10. We can see that the states near the Fermi level predominantly originate from of R f and Fe d states. For Sm_2Fe_{17}, there is an exchange splitting of about 2 to 3 eV in the Fe d states. Similar behavior is observed for $Sm_2Fe_{17}N_3$ and $Sm_2Fe_{17}C_3$. As shown in Figs. 8(a)–8(d), the spin-up Fe d states are fully occupied in the base compound. Upon introducing interstitial nitrogen or carbon atoms, the d states of Fe 18h and Fe 18f atoms hybridize with the p states of interstitial atoms. As can be seen in Figs. 8(a)–8(d), near Fermi level, the Fe 18f and Fe 18h DOSs for $Sm_2Fe_{17}N_3$ are relatively larger than in the base compound Sm_2Fe_{17}, which indicates the hybridization of these states with the interstitial nitrogen or carbon atoms. With N or C insertion, the majority-spin states at the 18h and 18f Fe sites are broadened, and the number of occupied spin-up electrons decreases. Furthermore, the minority-spin states shift towards lower energy and the number of spin-down electrons increases, resulting in a decrease in magnetic moments for these sites, as shown in Figs. 5(a) and 5(b). This observation is in agreement with previous studies [27,76]. Overall, the Fe

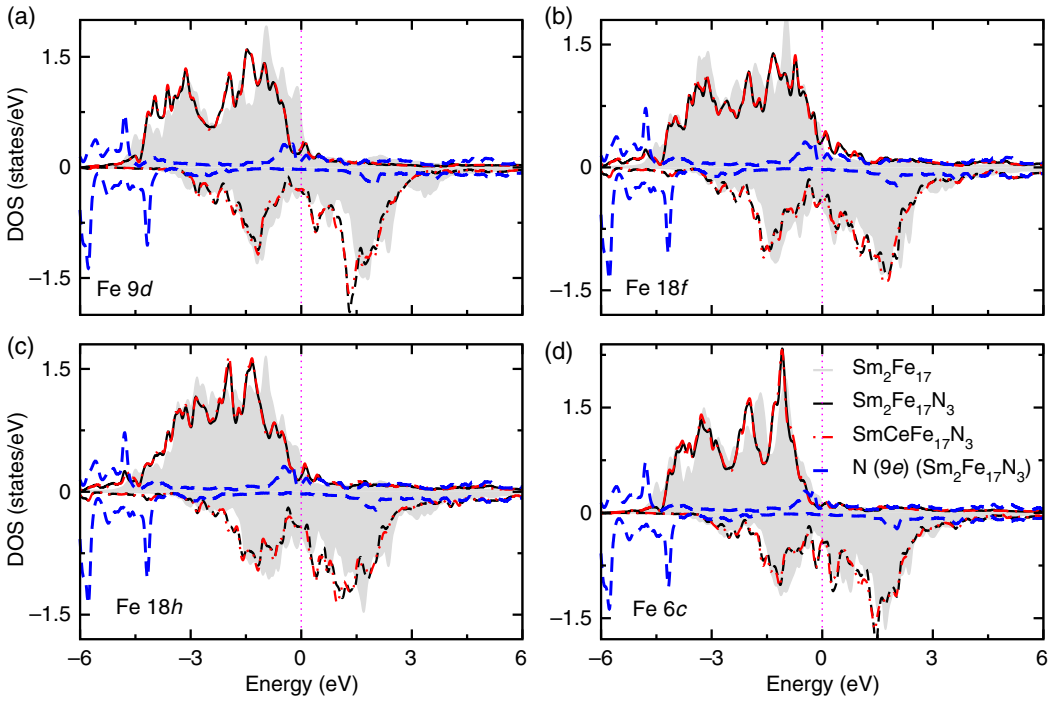

FIG. 8. The d-orbital DOS of crystallographically nonequivalent Fe atoms for Sm_2Fe_{17} (the gray filled area), $Sm_2Fe_{17}N_3$ (the black solid lines), and $SmCeFe_{17}N_3$ (the red dashed lines). (a)–(d) The $9d$, $18f$, $18h$, and $6c$ Fe sites, respectively. The p-orbital DOS for the $9e$ nitrogen interstitial atom in $Sm_2Fe_{17}N_3$ is also shown (the blue dotted lines). The spin-up and spin-down states are shown in the upper and lower halves of the panels, respectively.

moments are larger than that in pure Fe, which contributes to the excellent magnetic properties of these compounds.

As shown in Fig. 10(a), the R $4f$ states are not occupied in the spin-up channel and are partially occupied in the spin-down channel, confirming that the Sm moments align in the opposite direction as the Fe moments. The Sm DOS for Sm_2Fe_{17} calculated within only GGA + SOC (without U) is also shown in Fig. 10(a) (the blue dotted lines). As can be seen, without U, the Sm f orbitals form a narrow band which is pinned at the Fermi level (shown by the blue dashed line). The addition of U shifts the unoccupied spin-up f band towards the high energy. Also, the occupied spin-down band splits into lower and upper Hubbard bands, separated by roughly 6 eV. The exchange splitting at the Sm f states is similar to that of Fe d orbitals, even though the f DOS is substantially narrower. The Sm f orbital DOSs for base and nitrogen interstitial compounds are compared in Fig. 10(a). With N or C insertion, the f states shift to the lower-energy side. Since both the spin-up and spin-down states are pushed down to the lower energy, the change in magnetic moment is not as large as that at the Fe sites. The unoccupied f states are broadened by the insertion of N or C. The structure of the occupied f states remains more or less the same for all of the compounds.

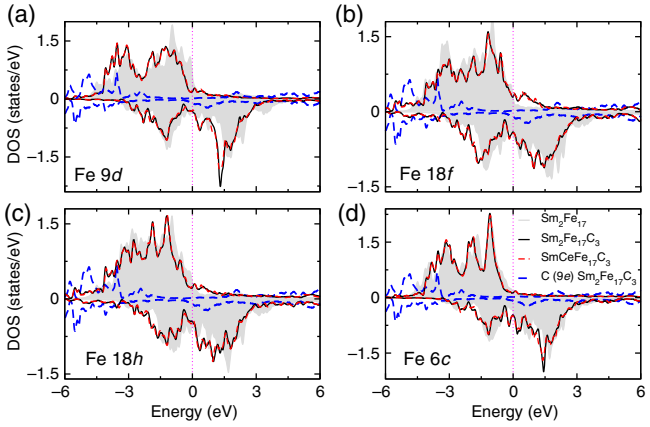

FIG. 9. The d-orbital DOS of crystallographically nonequivalent Fe atoms for Sm_2Fe_{17} (the gray regions), $Sm_2Fe_{17}C_3$ (the black solid lines), and $SmCeFe_{17}C_3$ (the red dashed lines). (a)–(d) The $9d$, $18f$, $18h$, and $6c$ Fe sites, respectively. The p-orbital DOS for the $9e$ carbon interstitial atom in $Sm_2Fe_{17}C_3$ is also shown (the blue dotted lines). The spin-up and spin-down states are shown in the upper and lower halves of the panels, respectively. The Fe DOS in $SmLaFe_{17}C_3$ exhibits similar characteristics and is not shown here.

To understand the effect of La or Ce substitution at the Sm sites on the magnetic properties of these compounds, we next analyze their electronic structure. The partial Fe d-DOS and the Sm f-DOS for the substituted systems are presented in Figs. 8(a)–8(d) and Figs. 10(b) and 10(c), respectively. Similar figures for carbon interstitial compounds are given in Figs. 9(a)–9(d) and Figs. 11(b) and 11(c). As can be seen, the Sm-La substitution has no effect on the Fe d-DOS, and the Fe DOS overlaps with an equivalent curve for $Sm_2Fe_{17}N_3/Sm_2Fe_{17}C_3$. This unaltered Fe DOS explains why the moments on Fe sites remain unchanged upon a Ce or La substitution. The only significant change in the DOS is at the R f states, which are shifted to higher energies by approximately 0.1 eV. For La- and Ce-substituted compounds, the peak of the Sm DOS near the Fermi level is reduced, with the reduction being higher for the La substitution. This reduction in the R DOS

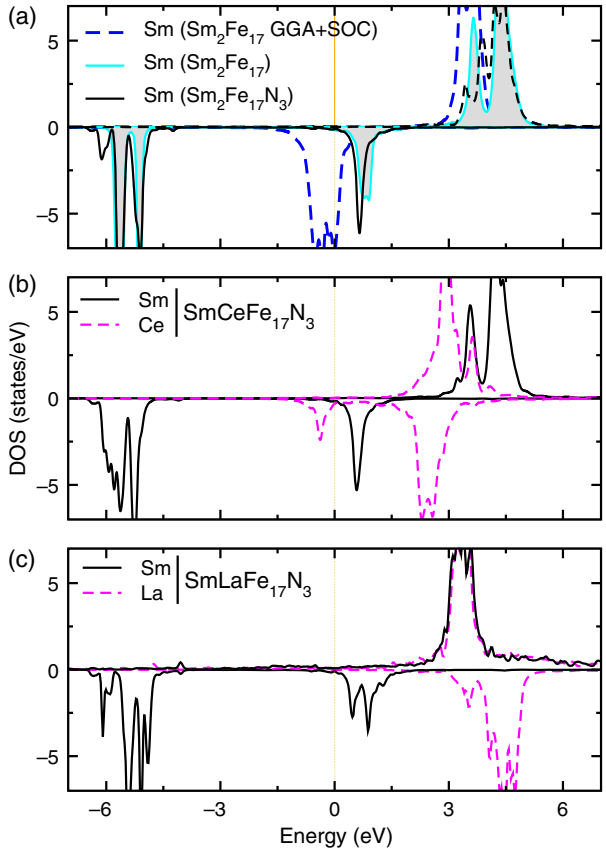

FIG. 10. The R $4f$ states DOS calculated with U_{Sm} as 6 eV. (a) Comparison of Sm $4f$ states in Sm_2Fe_{17} (the gray regions) and $Sm_2Fe_{17}N_3$ (the black solid lines). (b) The Sm (black solid lines) and Ce (magenta dashed lines) DOSs in $SmCeFe_{17}N_3$. Here, a U_{Ce} of 3 eV and a U_{Sm} of 6 eV is used. (c) The Sm (black solid lines) and La (magenta dashed lines) DOSs in $SmLaFe_{17}N_3$. The positive and negative portions represent spin-up and spin-down DOSs, respectively. The Sm f DOS from the GGA + SOC (without U) calculation is also shown in (a) as blue dotted lines.

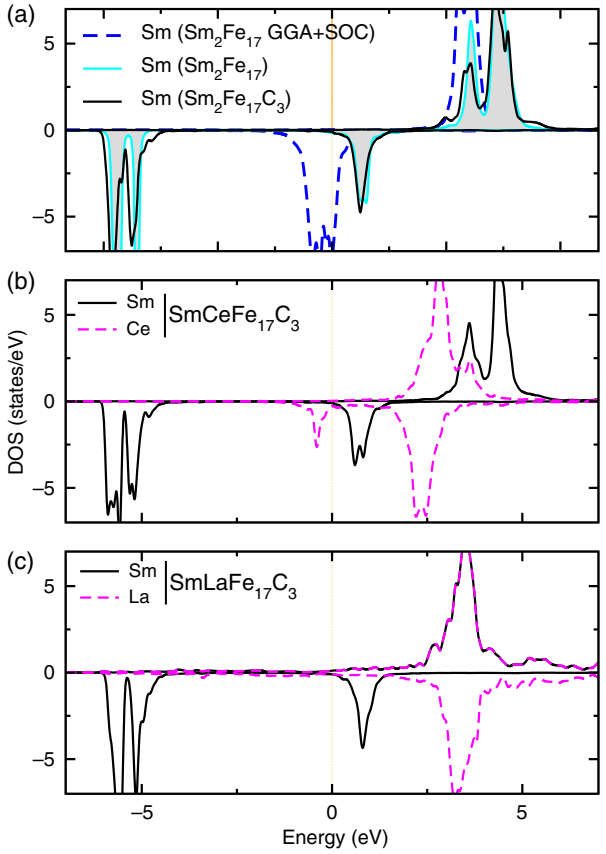

FIG. 11. The R $4f$ state DOS calculated with U_{Sm} at 6 eV. (a) Comparison of Sm $4f$ states in Sm_2Fe_{17} (the gray regions) and $Sm_2Fe_{17}C_3$ (the black solid lines). (b) The Sm (black solid lines) and Ce (magenta dashed lines) DOSs in $SmCeFe_{17}C_3$. Here, a U_{Ce} of 3 eV and a U_{Sm} of 6 eV is used. (c) The Sm (black solid lines) and La (magenta dashed lines) DOSs in $SmLaFe_{17}C_3$. The positive and negative portions represent spin-up and spin-down DOSs, respectively. The Sm f DOS from a GGA + SOC (without U) calculation is also shown in (a), as blue dotted lines.

is responsible for the reduction in the MAE seen with the La or Ce substitution. As the reduction in R DOS is more prominent for La-substituted compounds, the MAE for the La-substituted compounds shows a larger reduction (60%–70%) than for Ce-substituted compounds (40%–45%). The decrease in the MAE of $Sm_2Fe_{17}N_3$ on Ce substitution can also be explained by the difference in the prolaticity of R $4f$ electron clouds in Sm and Ce. As explained by Skomski and Sellmyer [75], because of a lesser number of electrons, the $4f$ electron clouds in Ce are in the shape of an oblate, whereas in Sm they take the shape of a prolate. Replacing a prolate ion (Sm, in this case) by an oblate ion tends to reduce the MAE.

Next, we estimate the effect of La or Ce substitution on the Curie temperature (T_C). In the Heisenberg model, the total energy of the system can be described as $E = \sum_{i,j} J_{ij} S_i S_j$. Here, S_i and S_j are the atomic spins on sites i and j, respectively, and J_{ij} is the exchange energy

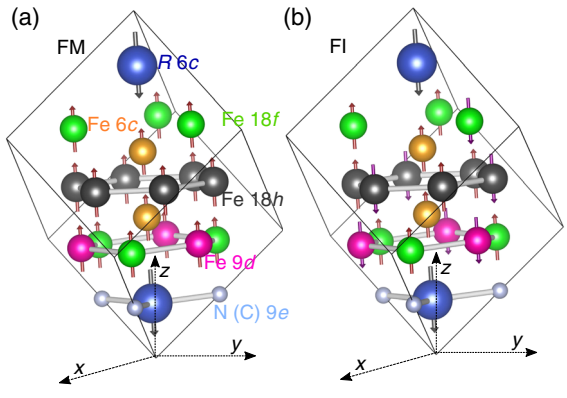

FIG. 12. Schematic defining the (a) ferromagnetic (FM) and (b) ferrimagnetic (FI) configurations of Fe atoms in the primitive cell used in the Curie-point calculations.

TABLE IV. The calculated energy difference (ΔE) between the FM state (where the spin moments on all the Fe atoms are aligned) and the AFM state (where the spin moments on the neighbors of the Fe atoms are antialigned) on a per-Fe-atom basis. The calculated mean-field Curie temperature ($\frac{1}{3}\Delta E$), along with the experimental Curie point, is also shown.

	Sm_2Fe_{17}	$Sm_2Fe_{17}N_3$	$SmLaFe_{17}N_3$	$SmCeFe_{17}N_3$	$Sm_2Fe_{17}C_3$	$SmLaFe_{17}C_3$	$SmCeFe_{17}C_3$
ΔE (meV)	−117.0	−264.7	−289.0	−306.7	−251.8	−256.5	−273.5
T_C (K)	453	1024	1117	1187	974	1024	992
T_C exp. (K)	390 [67]	749 [67]			680 [67]		

between these spins. For estimating J_{ij}, we calculate the energy difference between the ferromagnetic and antiferromagnetic structure (obtained by flipping the spin of most of the Fe nearest neighbors). These configurations are shown in Fig. 12. The resulting energy difference is listed in Table IV. In a mean-field approximation [77–79], the Curie temperature can be estimated as one third of this energy difference, measured on a per Fe basis. The base compounds Sm_2Fe_{17}, $Sm_2Fe_{17}C_3$, and $Sm_2Fe_{17}N_3$ show an energy difference (ΔE) of −117.0, −251.8, and −264.7 meV, respectively, between the FM and AFM states. This ΔE in the mean-field approximation, corresponds to T_C values of 453, 974, and 1024 K, respectively. Note that the mean-field Curie point is overestimated compared to the available experimental values. Upon substituting in La or Ce, the energy difference between the FM and AFM states increases by approximately 5%–9% for $Sm_2Fe_{17}C_3$, and by 9%–15% for $Sm_2Fe_{17}N_3$. The above analysis suggests that the mean-field exchange energy increases upon La or Ce substitution, which in turn will increase the Curie temperature. It is worth mentioning that, in the previous studies, the increase in Curie temperature of the base compound (Sm_2Fe_{17}) upon nitrogenation or carbonation has been attributed to an enhanced Fe-Fe interaction due to the expansion of the unit cell. This experimental observation is nicely reproduced by our calculations, where we see that the ΔE value for $Sm_2Fe_{17}C_3/Sm_2Fe_{17}N_3$ is more than 2 times larger than that for Sm_2Fe_{17}. We note that a mean-field approximation typically overestimates the transition temperature by around 20% or more, but it is useful in determining an upper limit for T_C. The T_C estimation could be further improved by atomistic spin-dynamics simulations [80,81] or within the random-phase approximation [82,83].

As introduced before, the main challenge with $Sm_2Fe_{17}N(C)_3$ compounds is their high-temperature stability, where they decompose to SmN and Fe. To address the stability issue, we calculate the formation energy (ΔE_f) of the nitrogen (carbon) vacancy in the pure ($Sm_2Fe_{17}N_3/Sm_2Fe_{17}C_3$) and La- or Ce-substituted compounds. The results are shown in Table V. To check the reliability of our results, formation energies are recalculated by including U for Sm and Ce atoms and by including spin-orbit coupling. The ΔE_f values show nominal changes in the formation energy upon the inclusion of U and SOC, as shown by $\Delta E_f(\mathrm{SOC}+U)$ in Table V. As we can see, for La- or Ce-substituted systems, N- or C-vacancy formation energy increases by about 20%–50% (depending upon the system). As the vacancy formation energies may be sensitive to the choice of lattice parameters, it is important to check the reproducibility of the trend in formation energy with optimized lattice parameters. However, doing it for all of the systems studied here is a computationally expensive task. Also, as mentioned before, the experimental volume for Ce variants of 2-17-3 compounds (i.e., $Ce_2Fe_{17}N_3$ and $Ce_2Fe_{17}C_3$) differs by only 0.5% compared to the Sm counterparts [84], but no information is present for the La version of these compounds. Here, to test the reliability of our calculations, we recalculate the nitrogen-vacancy formation energy with DFT-optimized lattices constants for $Sm_2Fe_{17}N_3$ and $SmLaFe_{17}N_3$. With the optimized lattice parameters for $Sm_2Fe_{17}N_3$, the nitrogen-vacancy formation energy found to be 1.02 eV, which is slightly lower than the value obtained with experimental lattice parameters. Similarly, for $SmLaFe_{17}N_3$, a calculation with optimized lattice parameters gives a nitrogen-vacancy

TABLE V. The calculated nitrogen- or carbon-vacancy formation energy (ΔE_f) for $Sm_2Fe_{17}X_3$, $SmLaFe_{17}X_3$, and $SmCeFe_{17}X_3$ (where X = N and C). ΔE_f and ΔE_f (SOC + U) denote the formation energy calculated without and with SOC + U, respectively. As can be seen, the La or Ce substitution enhances the N-vacancy formation energy by more than about 50% and C formation energy by approximately 60%.

ΔE_f	$Sm_2Fe_{17}N_3$	$SmLaFe_{17}N_3$	$SmCeFe_{17}N_3$	$Sm_2Fe_{17}C_3$	$SmLaFe_{17}C_3$	$SmCeFe_{17}C_3$
ΔE_f	1.18	1.60	1.85	0.53	0.77	0.90
ΔE_f (SOC + U)	1.20	1.64	1.81	0.52	0.79	0.88

formation energy of 1.27 eV. We note that, although with optimized lattice parameters the relative enhancement in the defect formation energy (25%) is slightly reduced compared to the one obtained with experimental lattice parameters (36%), it is still appreciably higher than for the base compounds. This enhanced vacancy formation energy indicates that La or Ce substitution may stabilize these compounds against nitrogen- (carbon)- vacancy formation at high temperatures.

IV. CONCLUSIONS

In conclusion, we use first-principles calculations in this paper to understand the magnetic properties of Sm_2Fe_{17}, $Sm_2Fe_{17}C_3$, and $Sm_2Fe_{17}N_3$ compounds. We show that, in the ground state of these compounds, the magnetic moments of R and Fe atoms prefer to antialign. The calculated magnetic properties of the base compounds agree well with the available experimental data. In agreement with the experimental reports, we find large uniaxial anisotropies for $Sm_2Fe_{17}C_3$ and $Sm_2Fe_{17}N_3$. In order to reduce the Sm content in these compounds, we further study the effect of La or Ce substitution for Sm on the magnetic properties. We show that, although La or Ce substitution in these compounds tends to reduce the MAE, it still maintains large uniaxial values. The La or Ce substitution reduces the total moment on the R site. This reduction of magnetic moments works effectively in terms of improving the total magnetization since the magnetic moments of R and Fe atoms antialign with each other. As a consequence of La or Ce doping, the exchange interaction energy increases, which in turn increases the Curie temperature. Furthermore, by calculating the N- or C-vacancy formation energy, we show that the La or Ce substitution improves the stability of these compounds at high temperatures against decomposition. Since all of the La- or Ce-substituted compounds have 50% less Sm content, they still maintain large axial anisotropy, a high Curie point, and large saturation magnetization, which makes them interesting prospects for permanent magnets with reduced critical rare-earth content. We hope this investigation will be helpful for experimental processes in making high-performance $Sm_2Fe_{17}C_3$, and $Sm_2Fe_{17}N_3$ magnets with less Sm content.

ACKNOWLEDGMENTS

This research is supported by the Critical Materials Institute, an Energy Innovation Hub funded by the U.S. Department of Energy, Office of Energy Efficiency and Renewable Energy, Advanced Manufacturing Office (T. P. and D. S. P). M. H. D was supported by the U.S. Department of Energy, Office of Science, Basic Energy Sciences, Materials Sciences and Engineering Division.

[1] K. Buschow, New developments in hard magnetic materials, Rep. Prog. Phys. **54**, 1123 (1991).
[2] K. H. J. Buschow and F. R. Boer, *Physics of Magnetism and Magnetic Materials* (Springer, New York, 2003).
[3] M. Kramer, R. McCallum, I. Anderson, and S. Constantinides, Prospects for non-rare earth permanent magnets for traction motors and generators, JOM **64**, 752 (2012).
[4] J. M. Coey, *Magnetism and Magnetic Materials* (Cambridge University Press, Cambridge, England, 2010).
[5] J. Coey, Hard magnetic materials: A perspective, IEEE Trans. Magn. **47**, 4671 (2011).
[6] J. Coey, Permanent magnets: Plugging the gap, Scr. Mater. **67**, 524 (2012).
[7] F. Bloch and G. Gentile, Anisotropy of the magnetization of ferromagnetic single crystals, Z. Phys. **70**, 395 (1931).
[8] H. Brooks, Ferromagnetic anisotropy and the itinerant electron model, Phys. Rev. **58**, 909 (1940).
[9] Z. Tie-Song, J. Han-Min, G. Guang-Hua, H. Xiu-Feng, and C. Hong, Magnetic properties of R ions in RCo_5 compounds (R = Pr, Nd, Sm, Gd, Tb, Dy, Ho, and Er), Phys. Rev. B **43**, 8593 (1991).
[10] W. Suski, N. Vityk, R. Gladyshevskii, A. Gilewski, T. Mydlarz, and K. Wochowski, Magnetic properties of $R_2Co_{17-x}Ga_x$ and $RCo_{5-x}Ga_x$ alloys (R = Y, Tb) in high magnetic fields, Chem. Met. Alloys **1**, 111 (2008).
[11] T. Shibata and T. Katayama, Magnetic properties of RCo_5 permanent magnets prepared by liquid phase sintering, Jpn. J. Appl. Phys. **12**, 1020 (1973).
[12] K. Konno, H. Ido, S. Cheng, S. Sankar, and W. Wallace, Al-substitution effects on the magnetic properties of RCo_5 (R = Y, Pr, Nd, and Sm), J. Appl. Phys. **73**, 5929 (1993).
[13] H. Tang, B. Shen, K. Buschow, F. De Boer, Y. Wang, and G. Qiao, Magnetic properties and structure of $R_2Co_{17-x}Ti_x$ intermetallic compounds (R = Pr or Nd), J. Appl. Phys. **81**, 5127 (1997).
[14] H. Xiu-Feng, J. Han-Min, W. Zi-Jun, T. Zhao, and C. Sun, Analysis of the magnetic properties of R_2Co_{17} (R = Pr, Nd, Sm, Gd, Tb, Dy, Ho, and Er), Phys. Rev. B **47**, 3248 (1993).
[15] D. Zhang, D. Middleton, E. Brück, F. De Boer, Z. Zhang, and K. Buschow, Magnetic properties of $R_2Co_{17-x}Ga_x$ compounds (R = Sm and Gd), J. Alloys Compd. **259**, 65 (1997).
[16] D. Givord, H. Li, and J. Moreau, Magnetic properties and crystal structure of $Nd_2Fe_{14}B$, Solid State Commun. **50**, 497 (1984).
[17] J. Holc, S. Beseničar, and D. Kolar, A study of $Nd_2Fe_{14}B$ and a neodymium-rich phase in sintered NdFeB magnets, J. Mater. Sci. **25**, 215 (1990).
[18] J. Coey, Intrinsic magnetic properties of compounds with the $Nd_2Fe_{14}B$ structure, J. Less-Common Met. **126**, 21 (1986).

[19] J. Coey, Comparison of the intrinsic magnetic properties of $R_2Fe_{14}B$ and $R(Fe_{11}Ti)$; R = rare earth, J. Magn. Magn. Mater. **80**, 9 (1989).
[20] W. Rodewald and W. Fernengel, Properties of sintered Nd-Fe-TM-B magnets, IEEE Trans. Magn. **24**, 1638 (1988).
[21] J. Herbst, $R_2Fe_{14}B$ materials: Intrinsic properties and technological aspects, Rev. Mod. Phys. **63**, 819 (1991).
[22] M. A. Susner, B. S. Conner, B. I. Saparov, M. A. McGuire, E. J. Crumlin, G. M. Veith, H. Cao, K. V. Shanavas, D. S. Parker, B. C. Chakoumakos *et al.*, Flux growth and characterization of Ce-substituted $Nd_2Fe_{14}B$ single crystals, J. Magn. Magn. Mater. **434**, 1 (2017).
[23] J. Coey and H. Sun, Improved magnetic properties by treatment of iron-based rare earth intermetallic compounds in anmonia, J. Magn. Magn. Mater. **87**, L251 (1990).
[24] H. Sun, Y. Otani, and J. Coey, Gas-phase carbonation of R_2Fe_{17}, J. Magn. Magn. Mater. **104–107**, 1439 (1992).
[25] H. Sun, J. Coey, Y. Otani, and D. Hurley, Magnetic properties of a new series of rare-earth iron nitrides: $R_2Fe_{17}N_y$ (y approximately 2.6), J. Phys. Condens. Matter **2**, 6465 (1990).
[26] H. Akai, M. Takeda, M. Takahashi, and J. Kanamori, Roles of light interstitials in magnetism of Fe, Solid State Commun. **94**, 509 (1995).
[27] L. Steinbeck, M. Richter, U. Nitzsche, and H. Eschrig, *Ab initio* calculation of electronic structure, crystal field, and intrinsic magnetic properties of Sm_2Fe_{17}, $Sm_2Fe_{17}N_3$, $Sm_2Fe_{17}C_3$, and Sm_2Co_{17}, Phys. Rev. B **53**, 7111 (1996).
[28] Y. Lu, O. Tegus, Q. Li, N. Tang, M. Yu, R. Zhao, J. Kuang, F. Yang, G. Zhou, X. Li *et al.*, Magnetic anisotropy of $(Sm, Y)_2Fe_{17}N_y$ compounds, Physica (Amsterdam) **177B**, 243 (1992).
[29] M. Katter, J. Wecker, L. Schultz, and R. Grössinger, Magnetocrystalline anisotropy of $Sm_2Fe_{17}N_2$, J. Magn. Magn. Mater. **92**, L14 (1990).
[30] K. Schnitzke, L. Schultz, J. Wecker, and M. Katter, High coercivity in $Sm_2Fe_{17}N_x$ magnets, Appl. Phys. Lett. **57**, 2853 (1990).
[31] G. B. Haxel, J. B. Hedrick, G. J. Orris, P. H. Stauffer, and J. W. Hendley II, U.S. Geological Survey Report No. 087-02, 2002.
[32] X. Kou, R. Grössinger, M. Katter, J. Wecker, L. Schultz, T. Jacobs, and K. Buschow, Intrinsic magnetic properties of $R_2Fe_{17}C_yN_x$ compounds: (R = Y, Sm, Er, and Tm), J. Appl. Phys. **70**, 2272 (1991).
[33] X. Kou, R. Grössinger, X. Li, J. Liu, F. De Boer, M. Katter, J. Wecker, L. Schultz, T. Jacobs, and K. Buschow, Magnetic phase transition and magnetocrystalline anisotropy of $Sm_2Fe_{17}C_xN_y$, J. Appl. Phys. **70**, 6015 (1991).
[34] P. Blaha, K. Schwarz, G. K. H. Madsen, D. Kvasnicka, and J. Luitz, *WIEN2K, An Augmented Plane Wave + Local Orbitals Program for Calculating Crystal Properties* (Technische Universität Wien, Vienna, 2001).
[35] E. Sjostedt, L. Nordstrom, and D. J. Singh, An alternative way of linearizing the augmented plane-wave method, Solid State Commun. **114**, 15 (2000).
[36] D. J. Singh and L. Nordstrom, *Planewaves Pseudopotentials and the LAPW Method*, 2nd ed. (Springer, Berlin, 2006).
[37] J. P. Perdew, K. Burke, and M. Ernzerhof, Generalized Gradient Approximation Made Simple, Phys. Rev. Lett. **77**, 3865 (1996); **78**, 1396(E) (1997).
[38] C. N. Christodoulou and T. Takeshita, Interstitial carbonation of the Sm_2Fe_{17} phase by reaction with hydrocarbons, J. Alloys Compd. **190**, 41 (1992).
[39] M. Katter, J. Wecker, C. Kuhrt, L. Schultz, and R. Grössinger, Structural and intrinsic magnetic properties of $Sm_2(Fe_{1-x}Co_x)_{17}N_y$, J. Magn. Magn. Mater. **114**, 35 (1992).
[40] C. Djega-Mariadassou, L. Bessais, A. Nandra, J. Grenèche, and E. Burzo, Structure and hyperfine properties of $Sm_2(Fe, Si)_{17}$, Phys. Rev. B **65**, 014419 (2001).
[41] B. C. Sales, B. Saparov, M. A. McGuire, D. J. Singh, and D. S. Parker, Ferromagnetism of Fe_3Sn and alloys, Sci. Rep. **4**, 7024 (2014).
[42] D. S. Parker, N. Ghimire, J. Singleton, J. Thompson, E. D. Bauer, R. Baumbach, D. Mandrus, L. Li, and D. J. Singh, Magnetocrystalline anisotropy in UMn_2Ge_2 and related Mn-based actinide ferromagnets, Phys. Rev. B **91**, 174401 (2015).
[43] T. N. Lamichhane, V. Taufour, M. W. Masters, D. S. Parker, U. S. Kaluarachchi, S. Thimmaiah, S. L. Bud'ko, and P. C. Canfield, Discovery of ferromagnetism with large magnetic anisotropy in ZrMnP and HfMnP, Appl. Phys. Lett. **109**, 092402 (2016).
[44] P. Larson, I. Mazin, and D. Papaconstantopoulos, Calculation of magnetic anisotropy energy in $SmCo_5$, Phys. Rev. B **67**, 214405 (2003).
[45] J.-X. Zhu, M. Janoschek, R. Rosenberg, F. Ronning, J. Thompson, M. A. Torrez, E. D. Bauer, and C. D. Batista, LDA + DMFT Approach to Magnetocrystalline Anisotropy of Strong Magnets, Phys. Rev. X **4**, 021027 (2014).
[46] J. P. Perdew and A. Zunger, Self-interaction correction to density-functional approximations for many-electron systems, Phys. Rev. B **23**, 5048 (1981).
[47] L. Petit, R. Tyer, Z. Szotek, W. Temmerman, and A. Svane, Rare earth monopnictides and monochalcogenides from first principles: Towards an electronic phase diagram of strongly correlated materials, New J. Phys. **12**, 113041 (2010).
[48] X.-W. Yan, Y. Wang, M. Gao, D. Ma, and Z. Huang, Magnetic and electronic properties of samarium-doped phenanthrene from first-principles study, J. Phys. Chem. C **120**, 22565 (2016).
[49] C. Morari, F. Beiuşeanu, I. Di Marco, L. Peters, E. Burzo, S. Mican, and L. Chioncel, Magnetism and electronic structure calculation of SmN, J. Phys. Condens. Matter **27**, 115503 (2015).
[50] F. Aryasetiawan, K. Karlsson, O. Jepsen, and U. Schönberger, Calculations of Hubbard U from first-principles, Phys. Rev. B **74**, 125106 (2006).
[51] V. I. Anisimov, I. Solovyev, M. Korotin, M. Czyżyk, and G. Sawatzky, Density-functional theory and NiO photoemission spectra, Phys. Rev. B **48**, 16929 (1993).
[52] A. Liechtenstein, V. Anisimov, and J. Zaanen, Density-functional theory and strong interactions: Orbital ordering in Mott-Hubbard insulators, Phys. Rev. B **52**, R5467 (1995).
[53] I. Solovyev, P. Dederichs, and V. Anisimov, Corrected atomic limit in the local-density approximation and the

electronic structure of *d* impurities in Rb, Phys. Rev. B **50**, 16861 (1994).
[54] E. R. Ylvisaker, W. E. Pickett, and K. Koepernik, Anisotropy and magnetism in the LSDA + *U* method, Phys. Rev. B **79**, 035103 (2009).
[55] M. Fähnle, K. Hummler, M. Liebs, and T. Beuerle, *Ab initio* electron theory for hard-magnetic rare-earth-transition-metal intermetallics, Appl. Phys. A **57**, 67 (1993).
[56] N. Drebov, A. Martinez-Limia, L. Kunz, A. Gola, T. Shigematsu, T. Eckl, P. Gumbsch, and C. Elsässer, *Ab initio* screening methodology applied to the search for new permanent magnetic materials, New J. Phys. **15**, 125023 (2013).
[57] E. Belorizky, M. Fremy, J. Gavigan, D. Givord, and H.-S. Li, Evidence in rare-earth (*R*)–transition metal (*M*) intermetallics for a systematic dependence of *R-M* exchange interactions on the nature of the *R* atom, J. Appl. Phys. **61**, 3971 (1987).
[58] J. Franse and R. Radwański, in *Handbook of Magnetic Materials*, Vol. 7, edited by K. H. J. Buschow (North-Holland, Amsterdam, 1993), p. 307.
[59] W. Körner, G. Krugel, and C. Elsässer, Theoretical screening of intermetallic $ThMn_{12}$-type phases for new hard-magnetic compounds with low rare earth content, Sci. Rep. **6**, 24686 (2016).
[60] S. Jaswal, W. Yelon, G. C. Hadjipanayis, Y. Wang, and D. J. Sellmyer, Electronic and Magnetic Structures of the Rare-Earth Compounds $R_2Fe_{17}N_{\xi}$, Phys. Rev. Lett. **67**, 644 (1991).
[61] In the previous DFT studies on $Sm_2Fe_{17}N_3$ and $Sm_2Fe_{17}C_3$, the *f* electrons were treated in the "open-core" approximation. This approximation does not allow direct hybridization of *f*-electron states with other valence-electron states. While the number of electrons in the 4*f* core is fixed to that of a free R^{3+} ion by charge-density constraint, the spin-density constraint fixes the magnetic spin moment of the 4*f* core to the value obtained from the *R-S* coupling.
[62] D. McNeely and H. Oesterreicher, Structural and low-temperature magnetic studies on compounds Sm_2Fe_{17} with aluminium substitution for iron, J. Less-Common Met. **44**, 183 (1976).
[63] J. Coey and D. Hurley, New interstitial rare-earth iron intermetallics produced by gas phase reaction, J. Magn. Magn. Mater. **104–107**, 1098 (1992).
[64] T. Iriyama, K. Kobayashi, N. Imaoka, T. Fukuda, H. Kato, and Y. Nakagawa, Effect of nitrogen content on magnetic properties of $Sm_2Fe_{17}N_x (0 < x < 6)$, IEEE Trans. Magn. **28**, 2326 (1992).
[65] O. Gutfleisch, Controlling the properties of high energy density permanent magnetic materials by different processing routes, J. Phys. D **33**, R157 (2000).
[66] S. Brennan, R. Skomski, O. Cugat, and J. Coey, Anisotropy of easy-plane Y_2Fe_{17}, $Y_2Fe_{17}N_3$ and Sm_2Fe_{17}, J. Magn. Magn. Mater. **140–144**, 971 (1995).
[67] S. T. Oyama, in *The Chemistry of Transition Metal Carbides and Nitrides*, edited by S. T. Oyama (Springer, New York, 1996), p. 1.
[68] Y. Otani, H. Miyajima, and S. Chikazumi, Magnetocrystalline anisotropy in Nd-Fe-B magnet, J. Appl. Phys. **61**, 3436 (1987).
[69] S. Miraglia, J. Soubeyroux, C. Kolbeck, O. Isnard, D. Fruchart, and M. Guillot, Structural and magnetic properties of ternary nitrides $R_2Fe_{17}N_x$ ($R \equiv$ Nd, Sm), J. Less-Common Met. **171**, 51 (1991).
[70] O. Isnard, S. Miraglia, J. Soubeyroux, D. Fruchart, and J. Pannetier, Neutron powder-diffraction study of Pr_2Fe_{17} and $Pr_2Fe_{17}N_{2.9}$, Phys. Rev. B **45**, 2920 (1992).
[71] M. Katter, J. Wecker, C. Kuhrt, L. Schultz, and R. Grössinger, Magnetic properties and thermal stability of $Sm_2Fe_{17}N_x$ with intermediate nitrogen concentrations, J. Magn. Magn. Mater. **117**, 419 (1992).
[72] X.-P. Zhong, R. Radwański, F. De Boer, T. Jacobs, and K. Buschow, Magnetic and crystallographic characteristics of rare-earth ternary carbides derived from R_2Fe_{17} compounds, J. Magn. Magn. Mater. **86**, 333 (1990).
[73] S. Buck and M. Fähnle, Rare-earth magnetic anisotropy: Is the crystal field theory valid?, J. Magn. Magn. Mater. **166**, 297 (1997).
[74] P. Larson and I. Mazin, Effect of lattice relaxation on magnetic anisotropy: Zr-doped Sm_2Co_{17}, Phys. Rev. B **69**, 012404 (2004).
[75] R. Skomski and D. Sellmyer, Anisotropy of rare-earth magnets, Journal of rare earths / Chinese Society of Rare Earths **27**, 675 (2009).
[76] M. Ogura, A. Mashiyama, and H. Akai, Role of N in the permanent magnet material $Sm_2Fe_{17}N_x$, J. Phys. Soc. Jpn. **84**, 084702 (2015).
[77] N. Ashcroft and N. Mermin, *Solid State Physics* (Saunders College Publishing, Philadelphia, 1976).
[78] W. Nolting and A. Ramakanth, *Quantum Theory of Magnetism* (Springer Science+Business Media, New York, 2009).
[79] P. W. Anderson, Theory of magnetic exchange interactions: exchange in insulators and semiconductors, Solid State Phys. **14**, 99 (1963).
[80] B. Skubic, J. Hellsvik, L. Nordström, and O. Eriksson, A method for atomistic spin dynamics simulations: Implementation and examples, J. Phys. Condens. Matter **20**, 315203 (2008).
[81] R. F. Evans, W. J. Fan, P. Chureemart, T. A. Ostler, M. O. Ellis, and R. W. Chantrell, Atomistic spin model simulations of magnetic nanomaterials, J. Phys. Condens. Matter **26**, 103202 (2014).
[82] L. Sandratskii and P. Bruno, Exchange interactions and Curie temperature in (Ga,Mn)As, Phys. Rev. B **66**, 134435 (2002).
[83] E. Şaşıoğlu, L. Sandratskii, P. Bruno, and I. Galanakis, Exchange interactions and temperature dependence of magnetization in half-metallic Heusler alloys, Phys. Rev. B **72**, 184415 (2005).
[84] According to the Inorganic Crystal Structure Database, the unit-cell volumes for $Ce_2Fe_{17}N_3$ and $Ce_2Fe_{17}C_3$ are 839.70 Å^3 and 828.98 Å^3, values which are quite close to the volumes for $Sm_2Fe_{17}N_3$ (838.01 Å^3) and $Sm_2Fe_{17}C_3$ (832.44 Å^3).
[85] See http://energy.gov/downloads/doe-public-access-plan.